Ultrasound in Med. & Biol., Vol. 33, No. 12, pp. 1859–1872, 2007
Copyright © 2007 World Federation for Ultrasound in Medicine & Biology
Printed in the USA. All rights reserved
0301-5629/07/$–see front matter

ELSEVIER

doi:10.1016/j.ultrasmedbio.2007.05.023

● *Original Contribution*

# SUBHARMONIC CONTRAST INTRAVASCULAR ULTRASOUND FOR VASA VASORUM IMAGING

David E. Goertz,*† Martijn E. Frijlink,* Dennie Tempel,* Vijay Bhagwandas,*‡ Andries Gisolf,‡ Robert Krams,* Nico de Jong,*†§ and Antonius F.W. van der Steen*†

*Biomedical Engineering Department, Erasmus Medical Centre, Rotterdam, The Netherlands; †Interuniversity Cardiology Institute of The Netherlands, Utrecht, The Netherlands; ‡Delft University of Technology, Delft, The Netherlands; and §Physics of Fluids, University of Twente, Enschede, The Netherlands

(*Received* 14 *March* 2007; *revised* 23 *May* 2007; *in final form* 24 *May* 2007)

**Abstract—The feasibility of subharmonic contrast intravascular ultrasound (IVUS) imaging was investigated using a prototype nonlinear IVUS system and the commercial contrast agent Definity™. The system employed a mechanically scanned commercial catheter with a custom transducer element fabricated to have sensitivity at both 15 and 30 MHz. Experiments were conducted at a fundamental frequency of 30 MHz (F30; 25% bandwidth), with on-axis pressures ranging from 0.12 to 0.79 MPa, as measured with a needle hydrophone. *In vitro* characterization experiments demonstrated the detection of 15 MHz subharmonic signals (SH15) when pressure levels reached 360 kPa. The formation of SH15 images was shown, with tissue signals suppressed to near the noise floor and contrast to tissue ratios were improved by up to 30 dB relative to F30. *In vivo* experiments were performed using the atherosclerotic rabbit aorta model. Following the bolus injection of contrast agent upstream of the imaging catheter, agent was detected within the aorta, vena cava and within the perivascular space. These results provide a first *in vivo* demonstration of subharmonic contrast IVUS and suggest its potential as a new technique for imaging vasa vasorum. (E-mail: goertz@sri.utoronto.ca)** **© 2007 World Federation for Ultrasound in Medicine & Biology.**

*Key Words:* **Intravascular ultrasound, Subharmonic, Nonlinear, Contrast agents, Microbubbles, Vasa vasorum, Atherosclerosis, Coronary artery, Vulnerable plaque.**

## INTRODUCTION

Intravascular ultrasound (IVUS) is an established clinical tool for assessing coronary artery atherosclerosis. Its use has contributed to an improved understanding of the natural history of atherosclerosis (Schoenhagen et al. 2001) and, increasingly, IVUS data are used as an endpoint in therapeutic trials (Nicholls et al. 2006). For diagnostic purposes, it is employed as an adjunct to angiography, to provide additional insight into the extent and severity of atherosclerosis and frequently reveals the presence of angiographically occult (*i.e.*, nonstenotic) lesions (Nissen and Yock 2001). Such "nonculprit" lesions are now recognized to be responsible for a high proportion of ensuing cardiac events resulting in either fatalities or requiring further interventional treatment (Glaser et al. 2005). A significant issue in cardiology is, therefore, to develop imaging methods to identify specific atherosclerotic lesions that are vulnerable to rupture (Schaar et al. 2004; Waxman et al. 2006). Candidate markers of lesion vulnerability currently under investigation include plaque morphology, volume, mechanical integrity and composition (Virmani et al. 2000, 2006). IVUS is well suited to indicate morphology and plaque burden, which has been the primary form of data analysis (Nissen and Yock 2001). Mechanical properties relevant to plaque vulnerability can be derived using IVUS elastography techniques (Schaar et al. 2003) and efforts are being made to perform radio-frequency (RF) IVUS signal analysis to gain insight into plaque composition (Nair et al. 2002). More recently, there is a growing recognition of the significance of vasa vasorum in plaque development and stability.

David E. Goertz is now at the Sunnybrook Health Sciences Centre and Department of Medical Biophysics, University of Toronto, Toronto, Ontario, Canada.

Address correspondence to: David E. Goertz, Rm C736b, Imaging Research, Sunnybrook Health Sciences Centre, 2075 Bayview Avenue, Toronto, Ontario, Canada, M4N3M5. E-mail: goertz@sri.utoronto.ca

The vasa vasorum are the microvascular bed responsible for nourishing the portion of the walls of arteries and veins that lie beyond the diffusion limit of the lumen (Williams and Heistad 1996). It is now well recognized that pathologic neovascularization occurs during plaque development and that the resulting microvessels have abnormal spatial distributions and branching patterns (Kwon et al. 1998; Zhang et al. 1993). Further, there is evidence suggesting that the spatial location of vasa vasorum may provide an indication of lesion vulnerability (Moreno et al. 2004). Neovascular vasa vasorum are part of an apparent positive feedback loop of inflammation and angiogenesis (Kumamoto et al. 1995; de Boer et al. 1999; Moulton et al. 2003) and are associated with intraplaque hemorrhage and, thereby, to rupture (Kologie et al. 2002; Milei et al. 1998). There is, therefore, considerable interest in targeting the neovascular vasa vasorum as a therapeutic strategy as well as to understand the potentially deleterious effects of other angiogenically active therapies may have on the plaque vasa vasorum (Moulton 2006). While imaging has been successful in detecting carotid artery vasa vasorum (Kerwin et al. 2003; Feinstein 2004), at present, there are no established methods of *in vivo* imaging vasa vasorum in coronary arteries.

IVUS is one candidate imaging modality for accomplishing this. Due to high levels of relative tissue-catheter motion, it is unlikely that conventional high frequency microvascular flow imaging methods (Kruse et al. 2002; Goertz et al. 2003) will be effective. IVUS in combination with microbubbles may be one approach for overcoming this issue. To date, IVUS imaging of contrast agents has been limited, with the focus being to enhance lumen boundary detection (Cachard et al. 1997) or to perform molecular imaging (Demos et al. 1999; Hamilton et al. 2004). There have been several reports of extra-luminal image enhancement following the bolus injection of contrast agent, which has been attributed to the presence of vasa vasorum (Carlier et al. 2005; Kakadiaris et al. 2006). While these results are promising, it has yet to be established that the enhancement is associated with perivascular microvessels. The basis of this approach is to compare postcontrast injection images with a baseline image derived from a single point in the cardiac cycle (O'Malley et al. 2005). The sensitivity and robustness of this approach ultimately relies upon the assumption of similarity between images acquired at the same point in the cardiac cycle and, as such, it is susceptible to acyclical catheter-vessel motion or nonuniform rotation velocity of the transducer element. This motivates the development of contrast IVUS detection techniques based on bubble-specific signatures, which are dominant at lower frequencies (de Jong et al. 2002).

To this end, a prototype nonlinear IVUS contrast imaging system has been developed in our laboratory (Goertz et al. 2006a). Using a conventional commercial 30 MHz catheter, its operation was evaluated *in vitro* with harmonic imaging of a 20 MHz transmit signal (H40) and subharmonic imaging of a 40 MHz transmit (SH20). The feasibility of improving contrast-to-tissue ratio (CTR) in H40 and SH20 modes relative to fundamental imaging was demonstrated with both free and targeted bubbles. These experiments were conducted *in vitro* with experimental micron to submicron sized agents. The feasibility of using harmonic IVUS contrast imaging to detect the vasa vasorum was shown (Goertz et al. 2006b) in atherosclerotic rabbit aortas with Definity™ (Bristol-Myers Squibb Medical Imaging, North Billerica, MA, USA). After activation, the agent was manipulated to preferentially retain smaller bubbles to improve its relative activity at higher frequencies (Goertz et al. 2006c). A significant enhancement was observed within the adventia following contrast injection, indicating the potential of harmonic IVUS as a new technique for imaging vasa vasorum.

While these *in vivo* results were encouraging, it is also of interest to improve the sensitivity of agent detection. With contrast harmonic imaging, transmit pressures are limited due to the effects of nonlinear propagation. Improvements in contrast-to-tissue ratio (CTR) with harmonic imaging may be achieved by improving transducer sensitivity and possibly through the use of alternative excitation methods (*e.g.*, Borsboom et al. 2003). Subharmonic imaging does not suffer from propagation artifacts (Shankar et al. 1998; Forsberg et al. 2000) and has recently been shown to detect microvascularity with an ultrasound biomicroscopy (UBM) system in mice using Definity™ (Goertz et al. 2005a). No subharmonic imaging of a clinically available agent with IVUS has been reported.

The objective of this study was to investigate the feasibility of *in vivo* subharmonic IVUS contrast imaging. The prototype system and catheter are first described and characterized. The generation of nonlinear signals from suspensions of Definity™ was examined for a 30 MHz transmit frequency. Phantom experiments were then performed to investigate image formation using frequency of 30 MHz (F30) and 15 MHz subharmonic signals (SH15). The *in vivo* feasibility was assessed in atherosclerotic rabbit aortas.

## IVUS SYSTEM DESCRIPTION

### *System overview*

The prototype nonlinear IVUS system employed in this study is similar that described in Goertz et al. (2006a). This system is an adapted version of one devel-

oped for tissue harmonic imaging (Frijlink et al. 2006a). An arbitrary waveform generator (AWG 520, Tektronix, Beaverton, OR, USA) was used to generate pulse sequences, which were amplified with a 60 dB gated linear power amplifier (LPI-10, ENI, Rochester, NY, USA). The amplified transmit signals were then bandpass filtered (5th order Butterworth 21 to 42 MHz) and sent through a modified commercial rotational motor unit (Du-Med, Rotterdam, The Netherlands) to a single element rotating IVUS catheter. On receive, the RF signals were amplified with a 44 dB preamplifier (AU-1263, Miteq, Hauppage, NY, USA), bandpass filtered (5th order Butterworth 8 to 60 MHz) and, then, digitized at 200 megasamples/s with a PC based 12-bit acquisition board (DP310 Acqiris, Geneva, Switzerland).

*Transducer*

The transducer employed in this study was a custom made element designed to have a dual frequency peak response, based on the approach described in Vos et al. (2005) and refined in Frijlink et al. (2006b). Whereas these studies used 20 and 40 MHz peaks, in this study, a design with peaks at 15 and 30 MHz was implemented. The dual peak tuning was achieved with the combination of a 76 micrometer thick active PZT (PPK22) layer and a 47 micrometer thick passive tin layer. The element was circular with a radius ($r$) of 0.4 mm and was mounted to a 4.3 French first generation commercial catheter (Princeps, Du-Med, Rotterdam, The Netherlands), replacing the original element.

*Transmit characteristics*

*Methods.* Subharmonic signals of a 30 MHz transmit pulse (25% −6 dB Gaussian envelope) were examined. A 30 MHz rather than the previously employed 40 MHz transmit was used, as it has been found that subharmonics become progressively more difficult to initiate from Definity™ as frequencies are increased beyond 30 MHz (Goertz 2002; Cheung et al. 2005). Experiments were conducted at a range of transmit pressures, which were measured with hydrophone water tank experiments. The hydrophone employed was a 0.075 mm diameter broadband (calibrated from 1 to 40 MHz) needle hydrophone (Precision Acoustics Ltd., Dorchester, UK). The relative hydrophone-transducer position was controlled by mounting the transducer to an XYZ micropositioning stage (MP 63 to 25-DC, Steinmeyer, Dresden, Germany). Peak negative pressures are reported.

An estimate of the frequency response of the IVUS transducer was made in the following manner. First, the hydrophone was situated along on the central beam axis at a distance ($z$) of 10 mm from the transducer face. The received signals from a sequence of narrowband pulses (10% −6 dB bandwidth Gaussian enveloped) with center frequencies ranging from 10 to 40 MHz was then acquired with 100 times averaging to improve the signal-to-noise ratio (SNR). The transmit voltages for all pulses were equal (as measured at the transmit amplifier output) and the peak on-axis pressure levels were kept below 150 kPa. At this distance, the Fresnel approximation ($z^2/r^2 \gg 1$) was considered to be valid (actual value 625) which simplifies the frequency ($f$) dependent relationship between the pressure at the transducer face ($p_o$) and far-field on-axis pressure ($p$) to (*e.g.*, Szabo 2004):

$$p(z, f) = \frac{p_o(f) \cdot \pi r^2 c}{zf} \tag{1}$$

where $c$ is the speed of sound in water. That is, at a fixed point along the beam axis, the pressure is inversely proportional to the frequency. The transmit frequency response of the catheter was, therefore, estimated from the measured far field frequency-dependent pressures by correcting for this diffraction relationship, frequency-dependent attenuation in water (0.00022 dB · MHz $^{-2}$ · mm$^{-1}$, *e.g.*, Bamber 2004), the frequency response of the hydrophone and by normalizing with respect to voltages measured at the input of the catheter. The end result is, therefore, a relative measure of the frequency response of the catheter and includes the combined effects of the transducer element and catheter cables.

One-dimensional on-axis beam profiles were then made at a range of transmit pressures using a step size of 100 $\mu$m. Peak negative pressures are reported. The transmit voltages, as measured at the catheter input with a 1 MOhm probe are also noted. The −6 dB pulse length and bandwidth for the transmit pulses were estimated using the hydrophone signals at 2.4 mm from the transducer.

Two-dimensional beam measurements of a plane perpendicular to the transducer face were performed using the lowest transmit voltage to estimate lateral beam widths and to align the transducer and hydrophone axes for the on-axis beam plots. These experiments were performed at center frequencies of 15 MHz and 30 MHz, with peak on-axis pressures kept below 150 kPa. A grid spacing of 50 micrometers laterally (parallel to the transducer face) and 200 micrometers axially (perpendicular to the transducer face) was employed. The peak of the envelope was estimated at each location.

*Transmit characteristics*

*Results.* The one-way transmit frequency response of the catheter is shown in Fig. 1. There is a pronounced peak at 16.0 MHz and a smaller one at 30 MHz, although the response is relatively flat (within several dB) between 24 and 40, with a small peak at 30 MHz.

Axial beam pressure plots for the 30 MHz case are

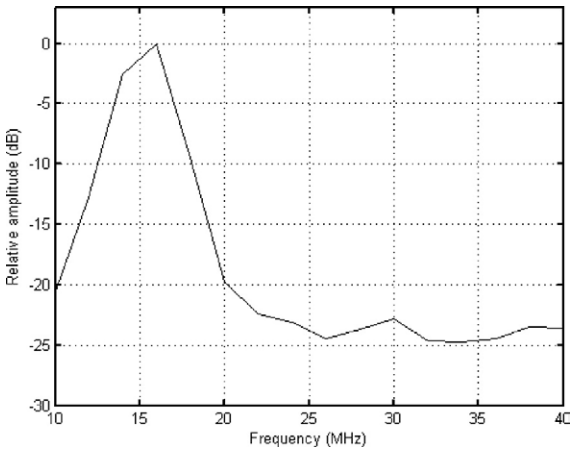


Fig. 1. One-way frequency response of catheter with custom dual frequency element. A pronounced peak in the vicinity of 15 MHz is evident.

shown in Fig. 2. for a range of transmit conditions. The curves exhibit peaks at approximately 2.2 to 2.6 mm and then undergo monotonic decays. In the remainder of this paper, the transmit pressure levels quoted will refer to the peak on-axis hydrophone values.

Two-dimensional beam cross-sections for transmit frequencies of 15 and 30 MHz are shown in Fig. 3. Each is normalized with respect to its peak on-axis pressure value, which occurs at 1.2 and 2.4 mm for 15 and 30 MHz, respectively. At these points, the −3 dB one-way beamwidths were 275 and 188 and −6 dB beamwidths were 275 and 405 micrometers respectively. The −6 dB axial resolution for the 30 MHz, as estimated from the pulse length at 2.4 mm, was 139 micrometers, which corresponded to a −12 dB bandwidth of 18%.

## PHANTOM AND AGENT CHARACTERIZATION EXPERIMENTS

### *Methods*

Phantom experiments were performed to investigate the production and detection of subharmonic signals from Definity™ with the prototype IVUS system and to form images based on signals acquired during mechanical scanning. The IVUS transducer was situated in a semicircular 1.4 mm diameter notch in the boundary between a suspension of agent and a block of tissue mimicking material (Goertz et al. 2006a).

The phantom material was produced according to the procedures detailed in de Korte et al. (1997) using 8% gelatin (Type A, Sigma Chemical company, St Louis, MO, USA), 2% agar-agarose (Agar-Agar CMN, Boom, Meppel, The Netherlands) and 1% carborundum powder with a particle size in the range of 3 to 10 $\mu$m (Cats Import, Hoogvliet, The Netherlands), all diluted with distilled water. Using this configuration, a single rotation of the catheter was sufficient to permit an analysis of received signals from both agent and tissue regions.

After agent activation using the Vialmix™ shaker (Bristol-Myers Squibb Medical Imaging, North Billerica, MA, USA), the vial was decanted for a period of 15 min, following the procedures described in Goertz et al. (2006c). This resulted in the preferential removal of larger bubbles, shifting the mean (volume weighted) bubbles size from 3.99 to 1.67 microns in diameter and eliminating 58% of the volume fraction of bubbles. The contrast agent was the diluted in Isotone II (Coulter Electronics, Luton, UK) by a factor of 3000 times relative to that in the vial. Experiments were performed at room temperature within 4 min after dilution.

Imaging was performed in the following manner. A pulse-inversion (PI) sequence (Hope-Simpson et al. 1999) was employed using equally spaced, alternately inverted pulses. Since relative motion between the tissue and transducer between pulses can result in decorrelation that will degrade the performance of PI suppression of fundamental frequency signals (Shen and Li 2002), it is desirable to minimize the spatial separation (*i.e.*, interpulse rotation angle) between pulses. Assuming there is a penetration depth of 10 mm, then, this imposes a 75 kHz limit in pulse repetition frequency (PRF). For a frame rate of 30 Hz, this corresponds to a maximum of 2500 pulses-per-rotation. In practice, RF power amplifier PRF limitations required a PRF of 17.5 kHz to be employed in this study. To evaluate the 2500 pulses per rotation condition, the frame rate was therefore reduced to 7 Hz.

SH15 image lines were calculated by first summing

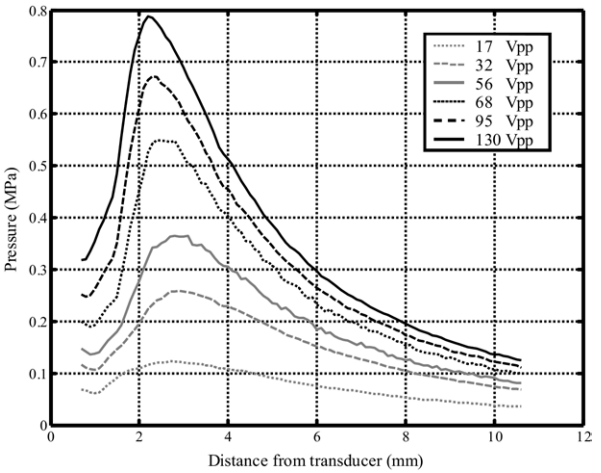


Fig. 2. On-axis peak negative pressure values for a range of 30 MHz pulse transmit amplitudes, as measured with a needle hydrophone in a water tank.

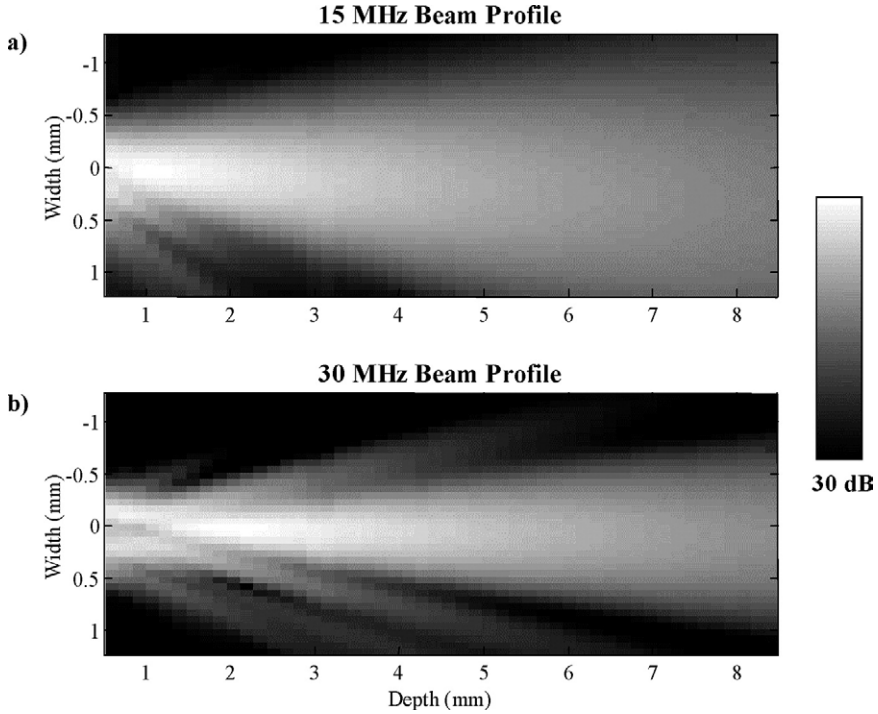


Fig. 3. Cross-sectional one-way two-dimensional beam profiles as measured with a needle hydrophone in a water tank for a transmit frequency of (a) 15 MHz and (b) 30 MHz.

eight adjacent pulses (*i.e.*, four adjacent inverted pulse-pairs), applying a digital bandpass filter (5th order Butterworth 8 to 20 MHz), and then calculating the envelope of the resulting signal. F30 image lines were calculated from the same data sets by averaging four alternate pulses (from the same eight pulse ensemble used for the SH15 image line), applying a digital bandpass filter (5th order Butterworth, 21 to 42 MHz) and, then, taking the envelope of the resulting signal.

*Data analysis*

The average tissue and agent spectra were estimated as a function of depth before image formation. Example results are shown for a depth window of 1 mm in length (1.3 $\mu$s duration), centered at 2.5 mm in depth. After the application of a Hanning window to each RF segment, the raw spectra were estimated with 700 traces from either the tissue or agent regions. Specifically, the average spectra of the 700 individual traces, and the average spectra of the 350 time-averaged pulse-pairs were calculated.

Following image formation, a quantitative analysis was performed for each transmit condition by calculating tissue-to-noise ratio (TNR), contrast-to-noise (CNR) and contrast-to-tissue ratio (CTR) within 1 mm depths windows centered at 1.5, 2.5, 3.5 and 4.5 mm. This was done in the following manner for both the F30 and SH15 images. For a given image, power was integrated within each 1 mm depth window and over 75 images lines (~90 degrees) in either tissue or agent regions. The calculations were also made for noise-only acquisitions. The resulting tissue, agent and noise power values were then used to estimate TNR, CNR and CTR. Finally, to provide an indication of the performance improvement in CTR associated with operating in subharmonic as opposed to fundamental mode, a parameter referred to as "CTR improvement" (Shen and Li 2003; Goertz et al. 2006a) was calculated as the ratio of CTR in harmonic mode over CTR in fundamental mode. The mean and standard error of these parameters were then calculated from eight independent images.

*Results*

*Received signals.* The average spectra from tissue and contrast regions (between 2 to 3 mm offset from transducer face) for the 0.55 MPa transmit case are shown in Fig. 4. In tissue, there was a pronounced peak at 30 MHz. With the application of PI, this was reduced by approximately 23 dB. In the contrast region, there was also a peak at 30 MHz, as well as a subharmonic peak in the vicinity of 15 MHz. Upon application of PI, the fundamental peak was reduced by 18 dB, while the subharmonic peak retained its original amplitude.

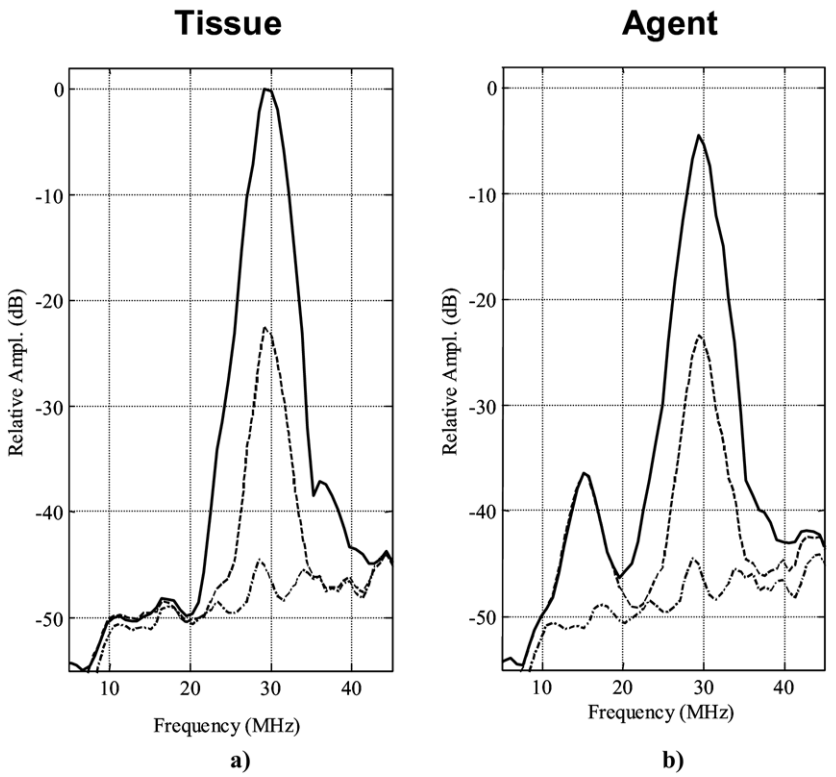


Fig. 4. Example received spectra from phantom experiments. Raw (solid line), pulse-inversion spectra (dashed line) and noise (dash-dot line) from the (a) tissue and (b) contrast agent regions for a 30 MHz transmit pulse (0.55 MPa, 2 to 3 mm depth). In both agent and tissue, the F30 signal is reduced with PI and in the agent, a substantial amount of SH15 signal is present and remains after pulse-inversion is applied.

*Imaging.* The results for F30 and SH15 image formation are shown for peak axial pressures of 250, 360, 550 and 670 kPa in Fig. 5a–d respectively. At all pressures, the F30 echoes from agent are similar in amplitude to those from tissue. In SH15 mode, the tissue signals are at or below the noise floor, with the exception of in the immediate vicinity of the catheter sheath where electronic saturation may occur. In SH15 mode, the contrast

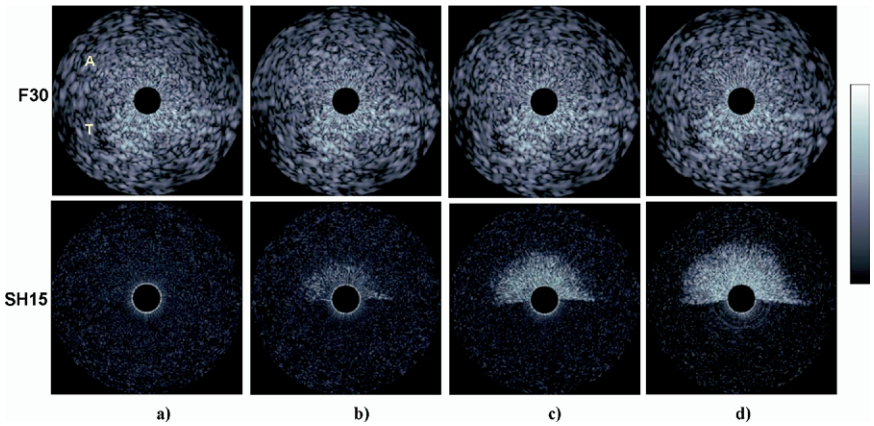


Fig. 5. Example images of phantom (bottom half -"T") and agent (upper half - "A") for F30 (top) and SH15 (bottom) as a function of transmit pressure. In all cases, the F30 image of agent appears slightly lower in amplitude than the tissue image. (a) At 250 kPa, the SH15 image the tissue is suppressed to the noise floor and no agent is detectable. (b) At 360 kPa, the agent can be detected in the vicinity of the catheter. (c) At 550 kPa, the agent is readily detectable while tissue signals are suppressed. (d) At 670 kPa, the SH15 image of contrast has increased in strength and is now visible to a depth of over 4 mm. Images are 12 mm in diameter. The display dynamic range is 40 dB.

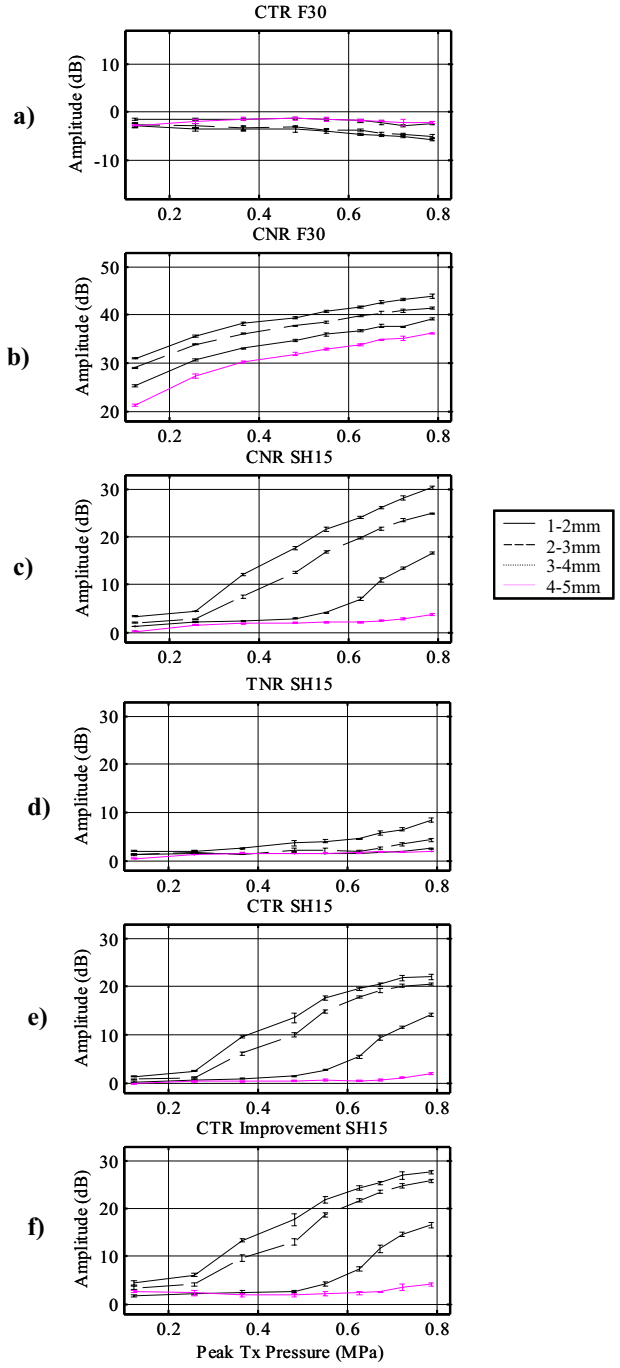


Fig. 6. Quantified image analysis as a function of transmit amplitude. F30 CTR (a) indicates agent signals are lower than that of tissue, although F30 CNR (b) increases as a function of transmit amplitude. SH15 CNR (c) increases as a function of transmit amplitude, while SH15 TNR (d) remains at the noise floor (1 to 2 mm case has catheter sheath artifacts). Both SH15 CTR (e) CTR improvement (f) demonstrate advantages for employing SH15 mode from the perspective of CTR.

agent images are below the noise floor until 250 kPa, but become clearly visible at higher pressures. When visible, the SH15 contrast signals decay to below the noise floor with increasing depth (*e.g.*, ~4 mm for 670 kPa).

A quantification of the F30 and SH15 imaging results is shown in Fig. 6a–f. It should be noted that for the 1 to 2 mm region, the presence of residual signals from the sheath echoes precludes a quantitative interpretation of this depth region. In Fig. 6a, F30 CTR curves were similar for all but the 4 to 5 mm case, which may be due to differences in attenuation between the phantom and agent. A small decrease in F30 CTR was also observed with increasing pressure. The F30 CNR increased with transmit pressure and decreased as a function of offset distance (Fig. 6b). In Fig. 6c, the SH15 CNR underwent a steady increase as a function of pressure for 1 to 2 and 2 to 3 mm. The increase with transmit pressure was delayed for the 3 to 4 mm distance and not evident for the 4 to 5 mm distance, which is consistent with the actual pressure levels being lower at the outer distances (Fig. 3). With the exception of the 1 to 2 mm distance, the SH15 TNR curves indicate that the tissue signals remained near the noise floor at all transmit pressures (Fig. 6d). As a result, the SH15 CTR followed a similar form to the SH15 CNR (Fig. 6e). The final plots of SH15 CTR improvements (Fig. 6f) have a similar form to the SH15 CTR, and reached a high in excess of 28 dB in the 1 to 2 mm case.

These data, therefore, indicate that SH15 IVUS imaging of Definity™ is feasible and improves the CTR relative to linear imaging.

## IN VIVO RABBIT AORTA EXPERIMENTS

### *Methods*

Initial experiments were conducted using the rabbit model of atherosclerosis to assess the feasibility of *in vivo* subharmonic IVUS. The procedures followed were similar to those reported in Goertz et al. (2006b). Atherosclerosis was initiated in the abdominal aortas of rabbits using a combination of endothelial cell injury procedures followed by an elevated cholesterol diet (Schaar et al. 2005). Imaging was performed 10 to 11 wk after initiating atherosclerosis. The experiments began with 3D IVUS imaging of the abdominal aorta using a pullback of a 40 MHz catheter with a Galaxy system (Boston Scientific Inc., Freemont, CA, USA). This was done to ascertain the presence and extent of the atherosclerotic plaque and the resulting images, referred to as "BSci40" images, were used to compare with subsequently acquired data from the prototype IVUS system. Following this, a 5 French agent delivery catheter with a helical release hole pattern was introduced through the carotid and its tip was situated approximately 1 cm

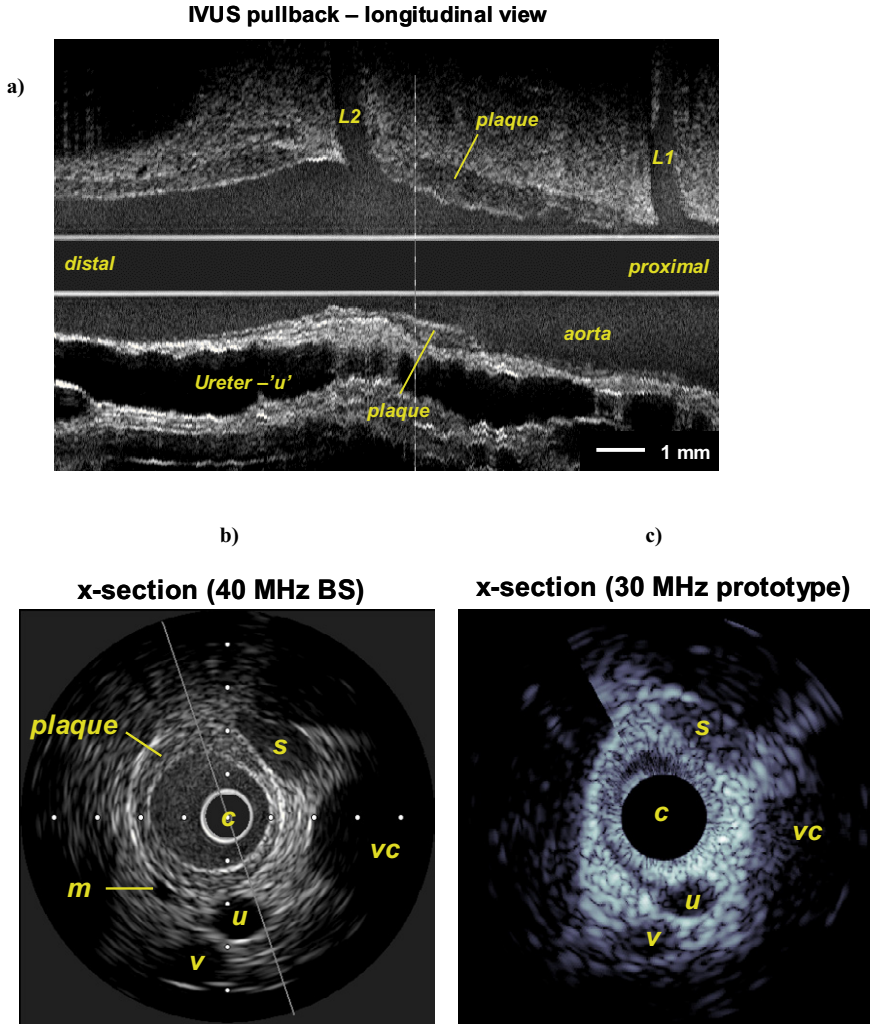


Fig. 7. (a) An example longitudinal section through a 3D BSci40 IVUS image of an atherosclerotic rabbit abdominal aorta. The plaque is evident, as well as two limbic artery branches (L1 and L2). b) A cross-sectional BSci image from the plane indicated in longitudinal section (1 mm between scale dots) clearly indicates an eccentric plaque, the vena cava (vc), a shunt vessel (s), a small vessel (m), a ureter (u) and another vessel (v). (c) A F30 prototype image (12 mm across) taken in this region shows several of these features (s, vc, u and v), albeit with degraded image quality.

below the lower renal artery branch point. The subharmonic IVUS catheter was then advanced through the femoral artery into the abdominal aorta and its transducer was located within 2 to 8 mm of a limbic artery branch point. This procedure was guided by angiography, with radiopaque contrast released proximally through the delivery catheter. The location adjacent to a limbic branch point facilitated the coregistration of the images with histology derived from tissue harvested from these locations.

IVUS imaging data were acquired with the catheter rotating at 7 Hz. The transmit power level employed corresponded to a peak on-axis water tank hydrophone pressure of 0.72 MPa. The data for every third image frame were acquired for a period of 60 s, beginning several seconds before the bolus release of contrast agent. The use of only every third image frame was necessary due to current acquisition limitations of the digitization board. Image processing was then performed as described in the previous section. Data sets were acquired following injections of 2.0 mL of saline diluted agent, released over 3 s. The agent concentration was 20% and was decanted for a period of 10 to 15 min, following the procedures described in Goertz et al. (2006c). Tissue was harvested to include a 2 cm section of aorta, vena cava and surrounding tissue. Serial histologic sectioning was performed every 0.25 mm and standard hematoxylin and eosin (HE) staining was conducted, as described in Goertz et al. (2006b). All experiments were performed in accordance with institutional

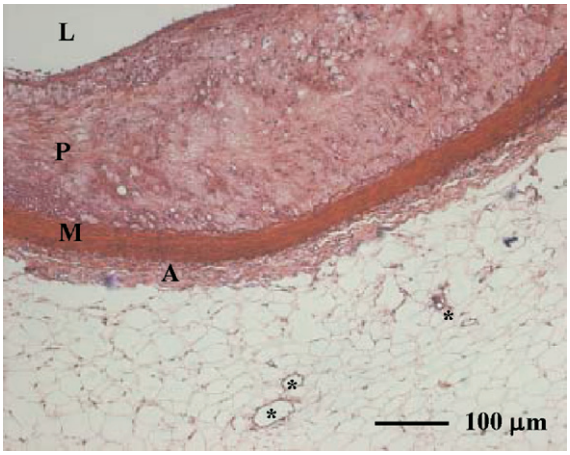


Fig. 8. A representative HE histologic section taken from the vicinity of the IVUS imaging plane. "L" is the aortic lumen, "M" the media, "P" the atherosclerotic plaque, and "A" the adventitia. Numerous adventitial microvessels are evident outside the media, some examples of which are denoted with an asterisk.

regulations and the "Guide for the Care and Use of Laboratory Animals" (National Research Council, 1996).

*Results*

An example longitudinal view of the BSci40 pullback data are shown in Fig. 7a, where the limbic artery branches and atherosclerotic plaque are evident. A cross-sectional image, taken in the vicinity of where the subharmonic imaging plane was located, is shown in Fig. 7b. The atherosclerotic plaque can be clearly demarcated as a slightly elliptical ring about the main lumen with a thickness ranging from 0.3 to 0.7 mm. The vena cava is also evident ("vc") along with several other vessels. "s" is a shunt vessel that, from an examination of the 3D data set, connects the immediately distal limbic artery to the vena cava, joining it at a point ~1 to 2 mm proximal to (*i.e.*, upstream of) the imaging plane. A small (~300 micron) microvessel "m" can also be seen 1 mm outside the aortic lumen at 7 o'clock. Two larger hypoechogeneic "vessels" can be seen, one of which ("u" at 5 o'clock) is thought to be a ureter and the outer ("v" at 6 o'clock) is a blood vessel. The F30 image from the prototype IVUS for this region is shown in Fig. 7c. While the image quality of the fundamental image has not been optimized, a number of common features can be observed, supporting that this is a similar location to that depicted with the BSci40 images, consistent with the angiogram guidance. Note also, that there is a slight under rotation of the catheter due to substantial levels of nonuniform rotation experienced by this older model catheter.

Histologic sections taken in the vicinity of this region confirm the presence of a concentric, elliptical plaque within the aorta. A representative example taken from the vicinity of the imaging plane is shown in Fig. 8. As previously observed with this animal model (Goertz 2006b), the plaque itself is avascular, while microvessels are present within the perivascular region. Note that we do not attempt to make specific correlations between the histology and contrast images, which is prohibited by uncertainly in the colocalization of the histology and imaging planes as well as by differences in their thicknesses and shapes.

An example series of F30 and SH15 images acquired following a contrast injection is shown in Fig. 9a–e. Figure 9a shows the F30 and SH15 images immediately before the release of contrast agent, where in the SH15 image the tissue signals are suppressed to near the noise floor. Shortly after the injection begins (~1 to 3 s), imaging was transiently obscured (not shown) due to the high attenuation levels associated with the passage of the bolus through the main lumen. By 3 s postinjection, F30 imaging has recovered in amplitude and a ring of enhancement is evident in the SH15 image arising from agent at the boundary of the aortic lumen. This feature was previously observed with harmonic imaging in phantoms and *in vivo* experiments (Goertz et al. 2006b) and is consistent with the effects of more slowly moving flow near the vessel boundary. A smaller vessel is also observed at 6 o'clock, consistent with the "m" vessel in the BSci40 images. Moreover, several faint and discrete enhancements appear to be within the adventitial region. At 5 s, the SH15 image (Fig. 9c) now shows a fading ring and agent within the shunt vessel "s". Immediately outside the ring, there is no enhancement, consistent with an avascular plaque. Of particular interest is that there are also a number of small discrete enhancements within the adventitial region just outside the hypoechogenic plaque region (*e.g.*, 8 to 11 o'clock). Histology revealed that microvessels were present in the adventitia, as also found in Goertz et al. (2006b). Following the convention employed in (Edelman et al. 1992) and (Herrmann et al. 2001), these data support the detection of vasa vasorum. By 7 s (Fig. 9d), the ring has faded indicating the clearance of the bolus from within the aortic lumen. The vessels "s" and "m" clearly have agent within and, additionally, there is now agent return evident in the vena cava. A number of small adventitial enhancements also persist. At 10 s (Fig. 9e), the main lumen was more homogeneously enhanced, consistent with the effects of agent recirculation. For a 2 kg rabbit, such as that employed in this study, this corresponds to an expected average blood recirculation time (defined as total volume/cardiac output; Schmidt-Nielsen 1984) of approximately 20 s. The observed arrival of recirculated agent is

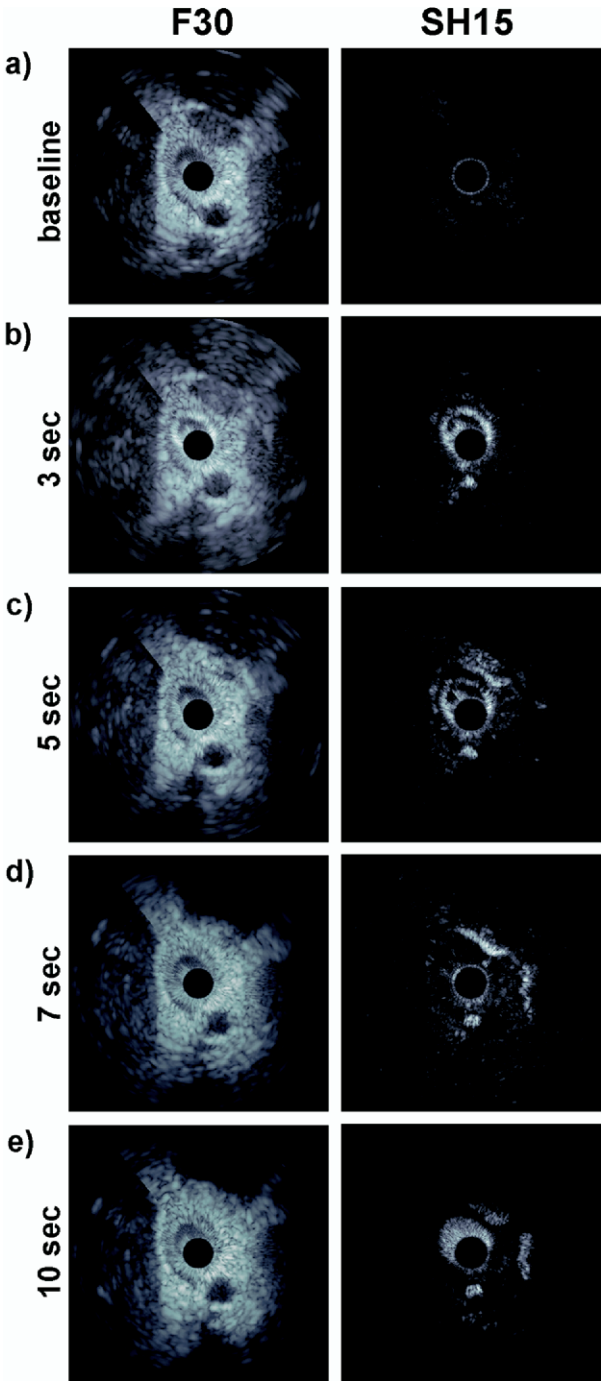


Fig. 9. Example *in vivo* results in an atherosclerotic rabbit aorta for F30 (left) and SH15 imaging (right). (a) Baseline image immediately before contrast release shows the tissue signals suppressed to near the noise floor in SH15 images. (b) By 3s postinjection, after the passage of the main bolus, a ring is present at the aortic lumen boundary, and adventitial enhancement is evident in the SH15 images. (c) At 5s, adventitial enhancement has increased, in a small vessel ("m" in Fig. 6b), the shunt ("s" in Fig. 6b) as well as in areas outside the lumen that are consistent with the location of vasa vasorum (*e.g.*, 8 to 11 o'clock). (d) Ring has faded and vena cava return is now apparent (3 o'clock). (e) Recirculation of agent is now evident as more homogenous enhancement within the aortic lumen. Images are 12 mm across; dynamic range is 40 dB.

earlier than this, as would be expected when it is released and imaged within a large vessel with high blood velocities. The recirculation time will be longer for larger animals (*e.g.* ~50 s for a 70 kg human) and the dilution ratio will be higher, both factors that will act to reduce this effect considerably.

## DISCUSSION

The agent characterization experiments showed that distinct subharmonic signals could be generated from a clinically available agent with an IVUS system. A threshold of detectable subharmonic occurrence was found to be between 250 to 360 kPa. These results are consistent with previous observations obtained with spherically focused PVDF UBM transducers at 20 MHz (Goertz et al. 2005; Needles et al. 2005) with Definity™ as well as an experimental lipid encapsulated agent at 30 MHz (Goertz et al. 2006d). Subharmonic threshold behavior is also observed with contrast agents at lower frequencies (Shi and Forsberg 2000; Sarkar et al. 2005) and with free bubbles (*e.g.*, Prosperetti 1977). Destruction effects were not examined in this study, but under similar conditions (30 MHz center frequency; 25% bandwidth) with another lipid encapsulated agent it was found to be present only at pressures in excess of 1.5 MPa, which are higher than those employed in this study.

The application of pulse-inversion to sequences to suppress fundamental frequency tissue signals in the context of mechanically scanned high frequency contrast imaging has been shown previously (Goertz et al. 2006a). Residual tissue signals in the fundamental frequency band can be attributed primarily to the decorrelation between successive pulses associated with transducer scanning. This has been analyzed in detail with simulations in Frijlink et al. (2006b). The degree of fundamental signal suppression with pulse-inversion during mechanical scanning can be improved by applying nonuniform weighting functions to the received pulses when processing (Frijlink et al. 2006c). It is also notable that the F30 suppression (Fig. 4) was less effective for the contrast agent than for tissue, which can be due to two factors. First, there may be residual energy left in the fundamental frequency bandwidth due to asymmetries in the bubble response during positive and negative pressure cycles (Morgan et al. 1998; Shen and Li 2003). In principle, this energy can also be exploited for the purposes of agent detection, although in the case of mechanical scanning, residual tissue signals in the fundamental frequency range will reduce the effectiveness of this approach. A second factor is that radiation pressure effects may be sufficient to induce bubble movement that will further degrade the performance of PI suppression of the transmitted signals.

The results of this study have shown the feasibility of *in vivo* subharmonic contrast IVUS imaging. Contrast agent was clearly detected within the main lumen, the vena cava and in small adventitial vessels. The results were consistent with the detection of vasa vasorum, which was previously achieved in this animal model using harmonic IVUS imaging (Goertz et al. 2006b). A quantitative comparison of the harmonic and subharmonic imaging has not been made here. In general, a primary advantage of subharmonic imaging over second harmonic imaging is the absence of propagation harmonics. The CNR depends on the agent behavior under particular conditions (frequency, bandwidth, pressure); in the present study a maximum of over 30 dB was reached. In Goertz et al. (2006a), it was found that subharmonic (SH20) imaging was superior to harmonic (H40) imaging in terms of CNR and CTR improvement.

In these experiments, a dual frequency transducer design was employed as a strategy to extend the transducer sensitivity over a wider bandwidth. This general approach has also been employed for the purposes of subharmonic imaging at lower frequencies (Takeuchi et al. 2003; Forsberg et al. 2004). In a previous report (Frijlink et al. 2006b), the use of 20 to 40 MHz design parameters resulted in two pronounced peaks in the vicinity of 20 and 40 MHz, with the 20 MHz peak being higher than the 40 MHz peak. In the present study, there is only a modest peak at the higher frequency (30 MHz) and the 15 MHz is 22 dB higher. A direct comparison between the two studies is not possible, since a different approach was taken in making the frequency response plots; whereby, in this study, we have accounted for the input voltage and made measurements in the far-field. Despite the lower relative efficiency at 30 MHz, sufficient transmit pressure (*i.e.*, up to 780 kPa) could still be generated to initiate subharmonic scattering and this could in principle be augmented through further increases in driving voltage. On receive, the CNR of SH15 signals will be directly dependent on the absolute sensitivity of the transducer in this frequency range and the relative sensitivity of the transducer in this range was high. The insertion loss was not measured but we note that the conventional commercial Du-med 30 MHz catheter was able to generate high pressures at 30 MHz (>2 MPa), but its efficiency dropped off significantly by 15 MHz (Frijlink et al. 2006a). A dual frequency approach may not be necessary if sufficient efficiency at these frequencies can be obtained with other transducer materials.

The effect of the IVUS transducer diffraction pattern on SH imaging also warrants comment. Given the threshold nature of subharmonic emissions (~250 to 360 kPa for Definity™ at these frequencies), SH imaging will be limited to the depth range over which pressure can be maintained above the threshold level. As can be seen in phantom experiments, SH detection range was limited to depths less than ~4 to 5 mm. As indicated by the on-axis hydrophone pressure measurements, diffraction effects are a primary factor in limiting the effective subharmonic imaging penetration depth. Attenuation in blood and vascular tissue (Lockwood 1991) will also be a factor *in vivo*. While 4 mm may be sufficient for most purposes, there are several possibilities for extending the subharmonic imaging depth. One is to increase the transmit voltage or transducer efficiency, although eventually, energy will be transferred up to higher harmonics through nonlinear propagation and may not result in improved subharmonics of the fundamental frequency. A second option would be to increase the aperture size of the transducer, since for a disc shaped element of radius $r$, the last local maximum for on-axis pressure occurs at $(r)^2$/wavelength. In the lateral direction, IVUS elements are constrained by catheter diameter considerations as well as circumferential resolution within the imaging plane. There is, therefore, arguably more flexibility in extending the element dimension along the catheter axis direction as a strategy for increasing penetration depth.

The spatial resolution in the lateral (circumferential) direction will be determined primarily by the overlap of the transmit and receive beams. While in a linear imaging system these will be identical, with subharmonic imaging, the effective resolution can be expected to be intermediate between the fundamental and subharmonic frequency beams (Fig. 3). As discussed in Goertz et al. (2005a) for a spherically focused beam, an additional effect is that the threshold nature of the subharmonics will act to decrease the lateral extent of the transmit beam where subharmonics will be detected, thereby improving the effective lateral width of the transmit beam. This issue was not examined in the present study. For any vascular imaging modality, the appearance of small vessels in an image is determined in large part by the spatial resolution of the system relative to the vessel sizes and spacing. Microvessels range in caliber from 5 up to 100 to 300 $\mu$m in diameter and reports of the vasa vasorum appear to fall within this range (Kwon et al. 1998; Herrmann et al. 2001). In the cases of clinical MRI and low-frequency contrast ultrasound, spatial resolution is typically on the order of a cubic millimeter and imaging voxels of this size will encompass a large number of microvessels that cannot be individually resolved. Consistent with this, the results of these modalities for carotid vasa vasorum imaging indicate a spatially diffuse enhancement outside the main lumen following contrast injection (Kerwin et al. 2003; Feinstein 2004). For the subharmonic IVUS system reported here, the resolution is on the order of larger microvessel diameters. Detected microvessels that are smaller than the voxel size will,

therefore, appear to be larger than their actual size, as shown previously in Goertz et al. (2003). While many microvessels will not be individually resolved, it is not clear if this will be detrimental to the clinical utility of this approach. Indeed, the relatively high spatial resolution of IVUS may be sufficient to map the distribution of neovascular "hot spots" that have been identified as being potentially linked to plaque vulnerability (Moreno et al. 2004).

At high ultrasound frequencies, another issue to consider is the number of microbubbles that are expected to be present within a voxel. As the resolution cell scales down with increasing frequencies the volume of blood and, therefore, number of microbubbles is also reduced. Taking the resolution cell in the present case to be on the order of 300 $\mu$m laterally and 150 $\mu$m in depth, this corresponds to a volume of approximately 10 nanolitres. If it is assumed that 10% of this is occupied by blood then on average it would contain only on the order of 1 nL of blood, a very small fraction of blood within the body. From this perspective, the nonlinear activity of smaller bubbles at high frequencies is advantageous, since they are present in higher number densities in Definity™ (Goertz et al. 2006c) and for a given injection volume will, therefore, be present in higher number densities in blood. The actual bubble concentration achieved within the vessel wall and perivascular space in the present application is not known, however the local release of agent proximal to the imaging sight is expected to have increased the agent concentration relative to that which could have been achieved through, for example, a systemic venous injection.

The absolute detection limits of the system in terms of vessel caliber were not established but will be determined not only by the agent concentration that can be achieved in a resolution cell but also by the sensitivity of the system. One aspect of this is the signal-to-noise ratio of the received nonlinear signals, which was improved through the use of a transducer with high sensitivity at the subharmonic frequency. Further improvements in transducer sensitivity can be expected to enhance detection performance. Other detection strategies also warrant investigation and may further improve sensitivity. Chirped excitation schemes for example, have shown promise when implemented at higher frequencies for nonlinear imaging (Williams et al. 2006).

This article has investigated the detection of "free" microbubbles with IVUS for the purposes of detecting vasa vasorum. An alternative strategy will be to employ targeted microbubbles for vasa vasorum detection within atherosclerotic plaques. One means of doing this may be to target neovascular endothelial cells through markers such as $\alpha_v\beta_3$. This approach has been previously demonstrated with targeted microbubbles for imaging neovascular endothelial cells in tumors (Ellegala et al. 2003). In the context of vasa vasorum imaging in atherosclerosis, it was shown with targeted nanoparticles in combination with magnetic resonance imaging (Winter et al. 2003). Imaging targeted bubbles in a nonlinear manner at high frequencies was shown to be possible in another study (Goertz et al. 2005b). In addition to vasa vasorum imaging, targeted contrast in combination with IVUS is also of interest to assess markers of inflammation (Hamilton 2004) and thrombus (Demos et al. 1999).

## CONCLUSIONS

This study has shown the feasibility of *in vivo* subharmonic contrast IVUS with a commercial contrast agent. Despite recent advances, a great deal remains unknown about the specific mechanisms of vasa vasorum involvement in the progression and instability of plaques. Within this context, IVUS contrast imaging is suitable for longitudinal studies of the role of vasa vasorum in pathogenesis of atherosclerosis as well as for preclinical therapeutic studies. Such experiments may be particularly relevant due to the lack of other techniques capable of *in vivo* high resolution monitoring of vasa vasorum and should also provide a foundation for understanding the potential role and limitations of contrast IVUS in future clinical applications. It is anticipated that they will conceivably have application to gain further insight into the natural history of atherosclerosis, the effects of novel therapeutic strategies and possibly as a marker of plaque vulnerability.

*Acknowledgments*—This work was financially supported by the Dutch Technology Foundation (STW). The agent was provided by Bristol-Myers Squibb Medical Imaging. The authors thank Gerrit van Dijk for his contribution to the construction of the customized catheter.

## REFERENCES

Bamber JC. Attenuation and absorption. In: Hill CR, Bamber JC, ter Haar GR, eds. Physical principles of medical ultrasonics. 2nd edition. Chichester, UK: Wiley, 2004:188–199.

Borsboom JMG, Chin CT, de Jong N. Nonlinear coded excitation method for ultrasound contrast imaging. Ultrasound Med Biol 2003;29:277–284.

Cachard C, Finet G, Bouakaz A, Tabib A, Francon D, Gimenez G. Ultrasound contrast agents in intravascular echography: An *in vitro* study. Ultrasound Med Biol 1997;23:705–717.

Carlier S, Kakadiaris A, Dib N, Nagavi M. Vasa vasorum imaging: A new window to the clinical detection of vulnerable atherosclerotic plaques. Curr Atheroscl Rep 2005;7:164–169.

Cheung K, Couture O, Bevan PD, Burns PN, Foster FS. The effect of bubble size distribution and driving frequency on the "subharmonic" response from Definity™ microbubbles. Proc IEEE Ultrason Symp 2005:850–853.

de Jong N, Bouakaz A, Ten Cate FJ. Contrast harmonic imaging. Ultrasonics 2002;40:567–573.

de Boer OJ, van der Wal AC, Teeling P, Becker AE. Leucocyte recruitment in rupture prone regions of lipid-rich plaques: A prominent role for neovascularization? Cardiovasc Res 1999;41:443–449.

de Korte CL, Cespedes EI, van der Steen AFW, Norder B, te Nijenhuis K. Elastic and acoustic properties of vessel mimicking material for elasticity imaging. Ultrasonic Imag 1997;19:112–126.

Demos SM, Alkan-Onyuksel H, Kane BJ, Ramani K, Nagaraj A, Greene R, Klegerman M, McPherson, DD. *In vivo* targeting of acoustically reflective liposomes for intravascular and transvascular ultrasonic enhancement. J Am Coll Cardiol 1999;33:867–875.

Edelman ER, Nugent MA, Smith LT, Karnovsky MJ. Basic fibroblast growth factor enhances the coupling of intimal hyperplasia and proliferation of vasa vasorum in injured rat arteries. J Clin Invest 1992;89:465–473.

Ellegala DB, Poi HL, Carpenter JE, Klibanov AL, Kaul S, Shaffrey ME, Sklenar J, Lindner JR. Imaging tumor angiogenesis with contrast ultrasound and microbubbles targeted to alpha. (v) beta 3. Circulation 2003;108:336–341.

Feinstein SB. The powerful microbubble: From bench to bedside, from intravascular indicator to therapeutic delivery system, and beyond. Am J Physiol 2004;287:H450–H457.

Forsberg F, Shi WT, Goldberg BB. Subharmonic imaging of contrast agents. Ultrasonics 2000;38:93–98.

Forsberg F, Shi WT, Jadidian B. Multi-frequency harmonic arrays: Initial experience with a novel transducer concept for nonlinear contrast imaging. Ultrasonics 2004;43:79–85.

Frijlink ME, Goertz DE, van Damme LC, Krams R, van der Steen AF. Intravascular ultrasound tissue harmonic imaging in vivo. IEEE Trans Ultrason Ferroelectr Freq Contr 2006a;53:1844–1852.

Frijlink ME, Goertz DE, Vos HJ, Tesselaar E, Blacquière G, Gisolf A, Krams R, van der Steen AFW. Harmonic intravascular ultrasound imaging with a dual-frequency catheter. Ultrasound Med Biol 2006b;32:1649–1654.

Frijlink ME, Goertz DE, de Jong N, van der Steen AFW. Pulse-inversion sequences for mechanically scanned transducers. IEEE Ultrason Symp 2006c;1286–1289.

Glaser R, Selzer F, Faxon DP, Laskey WK, Cohen HA, Slater J, Detre KM, Wilensky RL. Clinical progression of incidental, asymptomatic lesions discovered during culprit vessel coronary intervention. Circulation 2005;111:143–149.

Goertz DE. High frequency flow imaging of the microcirculation. 2002 PhD thesis, University of Toronto.

Goertz DE, Yu JL, Kerbel RS, Burns PN, Foster FS. High frequency 3D imaging of the microcirculation. Ultrasound Med Biol 2003;29:39–51.

Goertz DE, Cherin E, Needles A, Karshafian R, Duckett A, Burns PN, Foster FS. High frequency nonlinear b-scan imaging of microbubble contrast agents. IEEE Trans Ultrason Ferroelectr Freq Control 2005a;52:65–79.

Goertz DE, van Wamel A, Frijlink ME, de Jong N, van der Steen AFW. Nonlinear imaging of targeted microbubbles with intravascular ultrasound. IEEE Ultrason Symp 2005b;2003–2006.

Goertz DE, Frijlink ME, de Jong N, van der Steen AF. Nonlinear intravascular ultrasound contrast imaging. Ultrasound Med Biol 2006a;32:491–502.

Goertz DE, Frijlink ME, Tempel D, van Damme LC, Krams R, Schaar JA, Ten Cate FJ, Serruys PW, de Jong N, van der Steen AFW. Contrast harmonic intravascular ultrasound: A feasibility study for vasa vasorum imaging. Invest Radiol 2006b;41:631–638.

Goertz DE, Frijlink ME, de Jong N, van der Steen AFW. High frequency attenuation properties of Definity™ and modified Definity™ populations. IEEE Ultrason Symp 2006c (in press)

Goertz DE, Frijlink ME, de Jong N, van der Steen AFW. High frequency nonlinear scattering from a micrometer to submicrometer sized lipid encapsulated contrast agent. Ultrasound Med Biol 2006d;32:569–577.

Hamilton AJ, Huang SL, Warnick D, Rabbat M, Kane B, Nagaraj A, Klegerman M, McPherson DD. Intravascular ultrasound molecular imaging of atheroma components *in vivo*. J Am Coll Cardiol 2004;43:453–460.

Herrmann J, Lerman LO, Rodriguez-Porcel M, Holmes DR, Richardson DM, Ritman EL, Lerman A. Coronary vasa vasorum neovascularization precedes epicardial endothelial dysfunction in experimental hypercholesterolemia. Cardiovasc Res 2001;51:762–766.

Hope-Simpson D, Chin CT, Burns PN. Pulse inversion Doppler: A new method for detecting non-linear echoes from microbubble contrast agents. IEEE Trans Ultrason Ferroelectr Freq Control 1999;46:372–382.

Kakadiaris I, O'Malley S, Vavuranakis M, Carlier S, Hartley C, Metcalfe R, Mehran R, Naghavi M. Intravascular ultrasound-based imaging of vasa vasorum for the detection of vulnerable atherosclerotic plaque. J Am Coll Cardiol 2006;47:264A.

Kerwin W, Hooker A, Spilker M, Vicini P, Ferguson M, Hatsukami T, Yuan C. Quantitative magnetic resonance imaging analysis of neovasculature volume in carotid atherosclerotic plaque. Circulation 2003;107:851–856.

Kolodgie FD, Gold HK, Burke AP, Fowler DR, Kruth HS, Weber DK, Farb A, Guerrero LJ, Hayase M, Kutys R, Narula J, Finn AV, Virmani R. Intraplaque hemorrhage and progression of coronary atheroma. N Engl J Med 2002;349:2316–2325.

Kruse DE, Ferrara KW. A new high resolution color flow system using an eigendecomposition based adaptive filter for clutter rejection. IEEE Trans Ultrason Ferroelectr Freq Control 2002;49:1384–1399.

Kumamoto M, Nakashima Y, Sueshi K. Intimal neovascularization in human coronary atherosclerosis—its origin and pathophysiological significance. Human Pathol 1995;26:450–456.

Kwon HM, Sangiorgi G, Ritman EL, McKenna C, Holmes DR, Schwartz RS, Lerman. A Enhanced coronary vasa vasorum neovascularization in experimental hypercholesterolemia. J Clin Invest 1998;101:1551–1556.

Lockwood GR, Ryan LK, Hunt JW, Foster FS. Measurement of the ultrasonic properties of vascular tissues and blood from 35-65 MHz. Ultrasound Med Biol 1991;17:653–666.

Milei J, Parodi JC, Alonso GF, et al. Carotid rupture and intraplaque hemorrhage: Immunophenotype and role of cells involved. Am Heart J 1998;136:1096–1105.

Moreno PR, Purushothaman R, Fuster V, Echeverri D, Truszczynska H, Sharma SK, Badimon JJ, O'Connor WN. Plaque neovascularization is increased in ruptured atherosclerotic lesions of human aorta—Implications for plaque vulnerability. Circulation 2004;110:2032–2038.

Morgan K, Averkiou M, Ferrara K. The effect of the phase of transmission on contrast agent echoes. IEEE Trans Ultrason Ferroelectr Freq Control 1998;45:872–875.

Moulton KS, Vakili K, Zurakowski D, Soliman M, Butterfield C, Sylvin E, Lo KM, Gillies S, Javaherian K, Folkman J. Inhibition of plaque neovascularization reduces macrophage accumulation and progression of advanced atherosclerosis. Proc Nat Acad Sci 2003;100:4736–4741.

Moulton KS. Angiogenesis in atherosclerosis: Gathering evidence beyond speculation Curr Opinions Lipid 2006;17:548–555.

Nair A, Kuban BD, Tuzcu EM, Schoenhagen P, Nissen SE, Vince DG. Coronary plaque classification with intravascular ultrasound radiofrequency data analysis. Circulation 2002;106:2200–2206.

Needles A, Goertz DE, Karshafian R, Cherin E, Brown AS, Burns PN, Foster FS. High frequency subharmonic flow imaging of contrast agents. IEEE Ultrason Symp 2005;629–631.

Nissen SE, Yock P. Intravascular ultrasound—Novel pathophysiological insights and current clinical applications. Circulation 2001;103:604–616.

Nicholls SJ, Sipahi I, Schoenhagen P, Crowe T, Tuzcu EM, Nissen SE. Application of intravascular ultrasound in anti-atherosclerotic drug development. Nat Rev Drug Discov 2006;5:485–492.

O'Malley SM, Vavuranakis M, Naghavi M, Kakadiaris IA. Intravascular ultrasound-based imaging of vasa vasorum for the detection of vulnerable atherosclerotic plaque. Lecture Notes Comp Sci 2005;3749:343–351.

Prosperetti A. Application of the subharmonic threshold to the measurement of the damping of oscillating gas bubbles. J Acoust Soc Am 1977;61:11–17.

Sarkar K, Shi WT, Chatterjee D, Forsberg F. Characterization of ultrasound contrast microbubbles using in vitro experiments and viscous and viscoelastic interface models for encapsulation. J Acoustical Society of America 2005;118(1):539–550.

Schaar JA, de Korte CL, Mastik F, Strijder C, Pasterkamp G, Boersma E, Serruys PW, van der Steen AFW. Characterizing vulnerable plaque features with intravascular elastography. Circulation 2003; 108:2636–2641.

Schaar JA, Muller JE, Falk E, Virmani R, Fuster V, Serruys PW, Colombo A, Stefanadis C, Cassells SW, Moreno PR, Maseri A, van der Steen AFW. Terminology for high-risk and vulnerable coronary artery plaques—Report of a meeting on the vulnerable plaque, June 17 and 18, 2003, Santorini, Greece. Eur Heart J 2004;25:1077–1082.

Schaar JA, de Korte CL, Mastik F, van Damme LCA, Krams R, Serruys PW, van der Steen AFW. Three-dimensional palpography of human coronary arteries—*Ex vivo* validation and in-patient evaluation. Herz 2005;30:125–133.

Schmidt-Nielsen K. Scaling: Why is animal size so important. Cambridge: Cambridge University Press, 1984.

Schoenhagen P, Ziada KM, Vince DG, Nissen SE, Tuzcu EM. Relation of matrix-metalloproteinase 3 found in coronary lesion samples retrieved by directional coronary atherectomy to intravascular ultrasound observations on coronary remodeling. J Am Coll Cardiol 2001;38:297–306.

Shankar PM, Krishna PD, Newhouse VL. Advantages of subharmonic over second harmonic backscatter for contrast-to-tissue enhancement. Ultrasound Med Biol 1998;24:395–399.

Shen CC, Li PC. Motion artifacts of pulse inversion-based tissue harmonic imaging. IEEE Trans Ultrason Ferroelectr Freq Control 2002;49:1203–1211.

Shen CC, Li PC. Pulse-inversion-based fundamental imaging for contrast detection. IEEE Trans Ultrason Ferroelectr Freq Control 2003; 50:1124–1133.

Shi WT, Forsberg F. Ultrasonic characterization of the nonlinear properties of contrast microbubbles. Ultrasound Med Biol 2000;26:93–104.

Szabo TL. Diagnostic imaging from the inside out. Burlington, MA: Elsevier Academic Press, 2004.

Takeuchi S, Zaabi MRAA, Sato T. Ultrasound transducer with double-peak frequency characteristics for subharmonic imaging. Jpn J Appl Phys Pt 1 2003;42:3253–3254.

Virmani R, Kolodgie FD, Burke AP, Farb A, Schwartz SM. Lessons from sudden coronary death—A comprehensive morphological classification scheme for atherosclerotic lesions. Arteriol Thromb Vasc Biol 2000;20:1262–1275.

Virmani R, Burke AP, Farb A, Kolodgie FD. Pathology of the vulnerable plaque. J Am Coll Cardiol 2006;47:C13–C18.

Vos HJ, Frijlink ME, Droog E, Goertz DE, Blacquière Gisolf GA, de Jong N, van der Steen AFW. A 20-40 MHz ultrasound transducer for intravascular harmonic imaging. IEEE Trans Ultrason Ferroelectr Freq Control 2005;52:2418–2422.

Waxman S, Ishibashi F, Muller JE. Detection and treatment of vulnerable plaques and vulnerable patients: novel approaches to prevention of coronary events. Circulation 2006;114:2390–2411.

Williams JK, Heistad DD. Structure and function of vasa vasorum. Trends Cardiovasc Med 1996;6:53–57.

Williams R, Needles A, Cherin E, Burns PN, Foster FS, Leavens C, Sherar MD. Harmonic chirp imaging with ultrasound contrast agents at high frequency. IEEE Ultrason Symp 2006;228–231.

Winter PM, Morawski AM, Caruthers SD, Fuhrhop RW, Zhang HY, Williams TA, Allen JS, Lacy EK, Robertson JD, Lanza GM, Wickline SA. Molecular imaging of angiogenesis in early-stage atherosclerosis with alpha. (v) beta(3)-integrin-targeted nanoparticles. Circulation 2003;108:2270–2274.

Zhang Y, Cliff WJ, Schoefl GI, Higgins G. Immunohistochemical study of intimal microvessels in coronary atherosclerosis. Am J Pathol 1993;143:164–173.